Electronic Supplementary Material (ESI) for Catalysis Science & Technology.

Supporting Information

Operando XAS/Raman/MS monitoring of ethanol steam reforming reaction-regeneration cycles

Aline Ribeiro Passos,[*a,b] Camille La Fontaine,[a] Leandro Martins,[b] Sandra Helena Pulcinelli,[b] Celso Valentim Santilli [b] and Valérie Briois [a]

[a] Synchrotron SOLEIL, L'Orme des Merisiers, BP48, Saint Aubin, 91192 Gif-sur-Yvette, France.
[b] UNESP- São Paulo State University, Institute of Chemistry, Rua Professor Francisco Degni, 55, 14800-900 Araraquara, SP, Brazil.

*E-mail: alinepassos@lnls.br

EXPERIMETAL SECTION

Catalyst Preparation. The Co/Al_2O_3 catalysts were prepared by incipient wetness impregnation of alumina samples (provided by Strem Chemicals, surface area 264 m^2g^{-1} determined by BET) to achieve an overall cobalt loading of 10 wt%. In a typical synthesis procedure, 0.99 g of hexahydrated cobalt nitrate nitrate (Sigma-Aldrich, 99.99% purity) were dissolved in 40 mL of distilled water. 2 g of alumina were added to the solution and the excess of water was removed in a rotary evaporator. Subsequently, the catalysts were dried at 100 °C for 4 h and calcined during 4 h at 450 °C under air.

Catalytic Test. The catalyst activation and ESR reaction were monitored *in situ* by time-resolved quick-XAS using a dedicated cell [1] connected to the gas feeding system installed on the ROCK beamline.[2] Quick-XAS measurements were performed in transmission mode using the SOLEIL home-made quick-EXAFS monochromator described in [3]. The Si (111) channel-cut crystal was tuned to a Bragg angle of 13.9° near to the Co K-edge energy (7709 eV). A channel-cut oscillation around 13.9° of 2.2° amplitude and with a frequency of 2 Hz was used allowing us to obtain four XAS spectra per second (two XAS spectra with decreasing angle and two ones with increasing angle). Spectra collected with upward Bragg angles and previously interpolated in a common energy grid from 7580 to 8500 eV were merged to improve the signal-to-noise ratio leading to a time resolution of 10 s per presented spectrum for *operando* monitoring of catalysts. Normalization of the XAS data was performed by using the Python normal_gui graphical interface developed at SOLEIL for the fast handling of the Quick-XAS data.[4] The proportion of the different cobalt species was determined by a multivariate data analysis, the so-called MCR-ALS method. Details about the use of the MCR-ALS method can be found in [5–7]. The EXAFS signal extraction and further Fourier transformation of the EXAFS spectra of pure chemical species determined by MCR-ALS were done using the Athena graphical Interface software.[8]

The cavity of the sample holder (2 mm thick) was filled with the powdery catalyst (23 mg).[1] The *in situ* catalyst activation was performed by heating the cell from room temperature to 500 °C under H_2 flow (12 mL min^{-1}) followed by 2 h of isothermal treatment. The activity to ESR and selectivity to products were measured at 500 °C. The reactant mixture (water/ethanol vapor molar fraction ratio of 6) was fed to the reactor with 40 mL min^{-1} of He through a saturator at 45 °C. The amounts of water and ethanol were set to provide liquid phase mole fraction of 0.96 (water/ethanol) and a gas phase molar fraction of 6 at 45 °C. It is noteworthy that before the

reaction the reactor was by-passed in order to fill the inlet gas line by the ESR gas feed as close as possible to the cell but also to measure the inflowing reaction mixture atmosphere. The ratio of ethanol to water was analyzed at the end of the experiment presented herein again by-passing the reactor, and we measured that ethanol and water proportions achieve the same level that before the reaction (Fig. S1). Nevertheless, a time for letting gases travelling to the cell and then to mass spectrometer (~ 3m 1/8' tube length) has to be taken into account when the valve was switched on, together with a dilution effect from the former gas loaded the cell. This explains that stable conditions at the mass spectrometer is only observed after several minutes after switching on the inlet valve. For the regeneration, 5 mL min^{-1} of 5% of O_2/He was added to the already circulating 40mL min^{-1} He flow saturated by the reactant mixture (vapor of water/ethanol molar fraction ratio of 6). The gas composition after reaction was continuously monitored by an online quadrupole mass spectrometer (Cirrus, MKS). The gas outlet composition was calculated from the mass spectrometer signal at m/z ratios of 44, 43, 31, 28, 26, 17, 16, 15, 2 for CO_2, CH_3CHO, CH_3CH_2OH, CO, C_2H_4, H_2O, O_2, CH_4, and H_2, respectively. *Operando* Raman monitoring of the catalyst during ESR was performed with a Raman RXN1 spectrometer (Kaiser Optical Systems, Incorporation, (KOSI)) using the 532 nm exciting line of a diode pumped solid state laser, the average resolution was 2 cm^{-1}, one spectra was recorded every 2 min. To allow the laser to impinge the sample surface, a 25 μm thick mica window is used for facing the long working distance objective (150 mm) used to focus the 532 nm excitation.

Then the 1st ESR followed by the 1st OX was also performed in a fixed-bed reactor at atmospheric pressure. The reaction products were analyzed online using a gas chromatograph (GC) unit equipped with a TCD and FID detector. HP PLOT Q (Agilent) column was used.

***Ex situ* characterization.** High resolution scanning electron microscopy was carried out in a FEI Inspect F50 microscope operated at 30 kV in transmission mode with STEM detector (STEM). A few droplets of the sample suspended in ethanol were placed on a carbon-coated copper grid. The mean value of particle size was statistically calculated by the measurement of 100 uniform particles in several selected STEM images

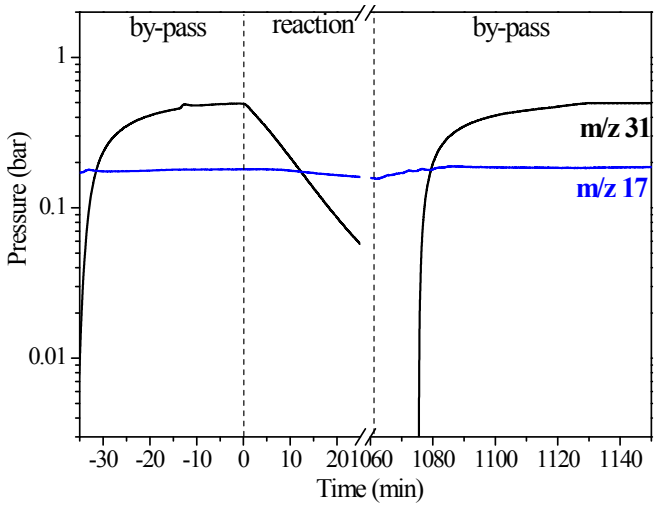

Fig. S1 Mass signal for ethanol (m/z 31) and water (m/z 17) before and after the reaction by-passing the reactor.

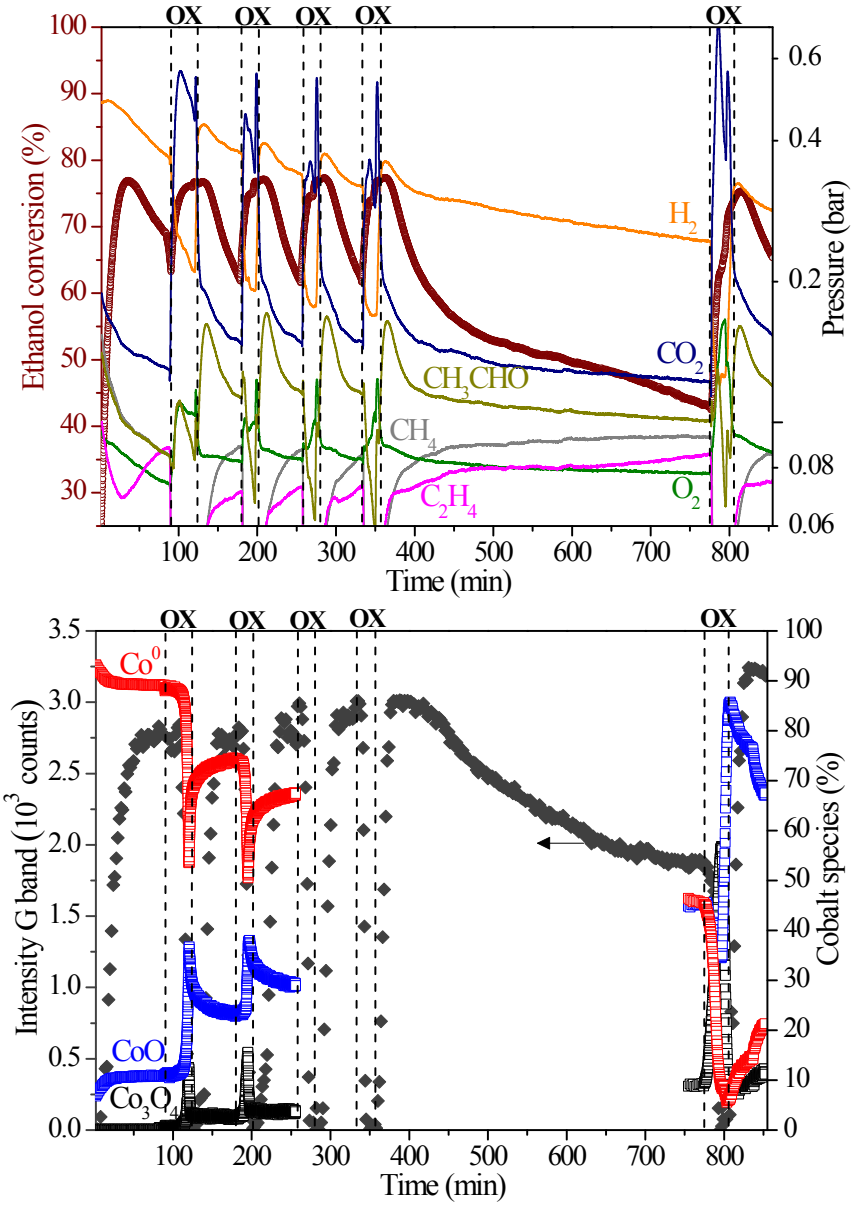

Fig. S2 Evolution of (a) ethanol conversion and reaction products monitored by Mass Spectrometry (logarithmic scale) (b) percentages of cobalt species determined by MCR-ALS during the catalyst ESR-OX cycles and intensity of Raman G line (diamond symbols). Conditions: ESR: water/ethanol ratio = 6, 40 mL min^{-1} of He. OX: 5mL min^{-1} of 5% O_2/He was added to 40 mL min^{-1} of He saturated by the water/ethanol vapor.

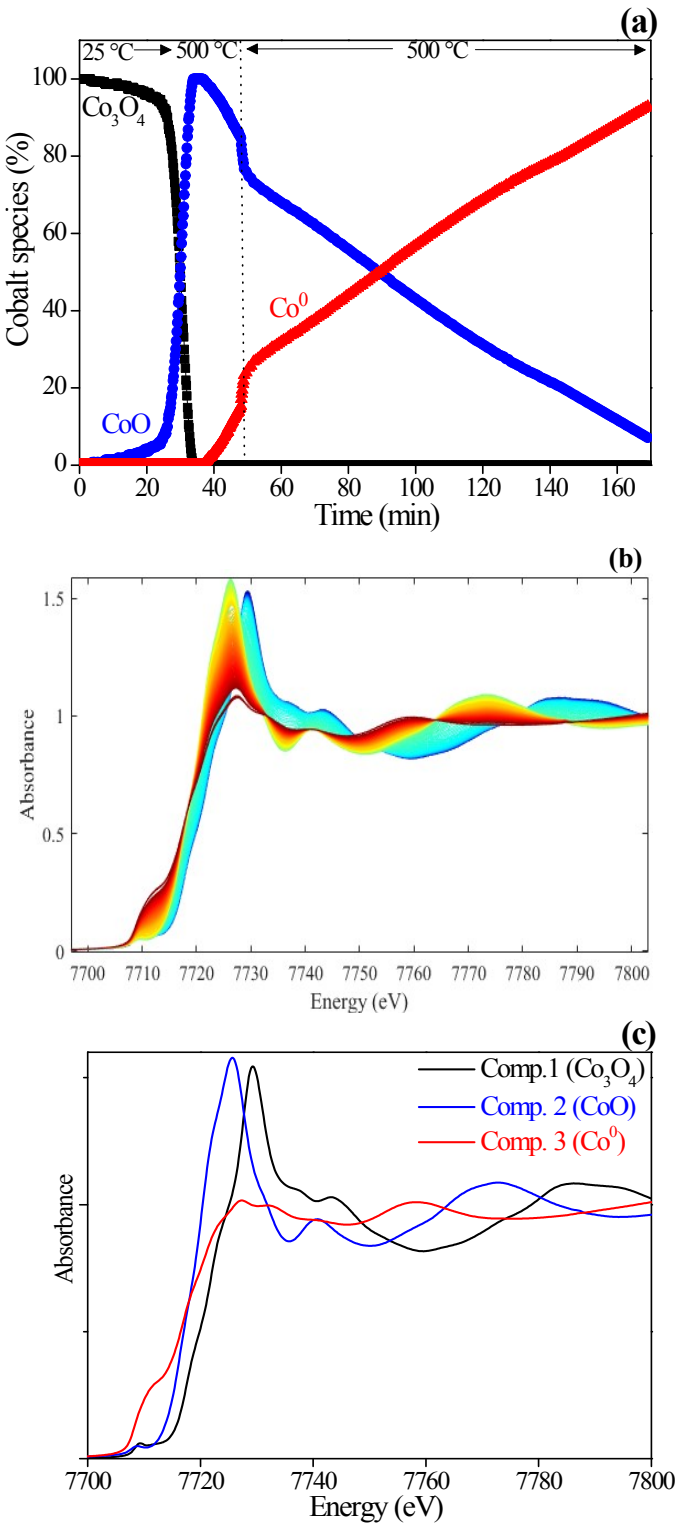

Fig. S3 Evolution of (a) percentages of cobalt species determined by MCR-ALS analysis of the time resolved Co K edge data presented in (b); (b) XANES spectra collected during the catalyst activation under H_2 from RT (deep blue color) to 500 °C (deep red color) and (c) pure spectral components determined by the MCR-ALS minimization.

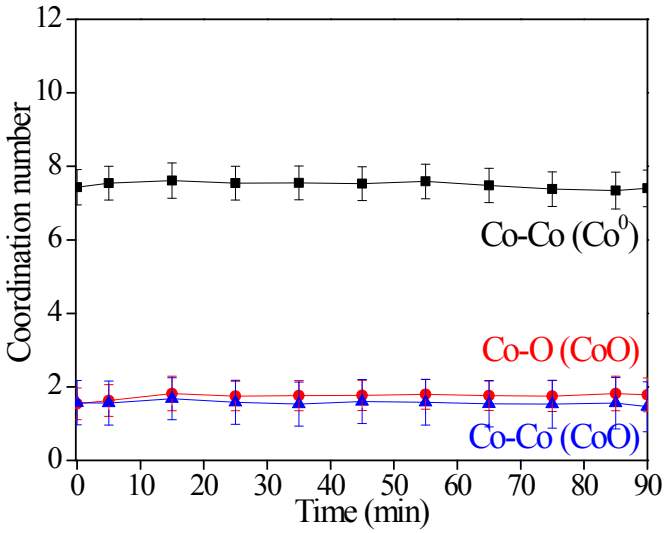

Fig. S4 Evolution of coordination numbers determined by EXAFS fittings during the first ESR reaction.

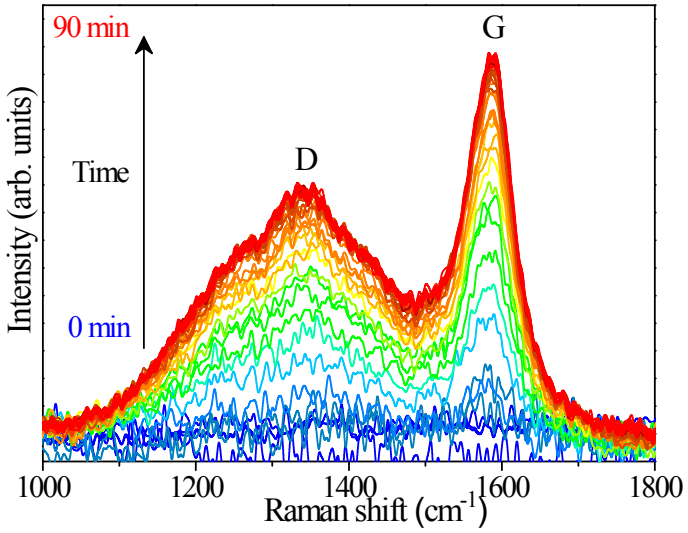

Fig. S5 Evolution of Raman spectra during the first ESR reaction.

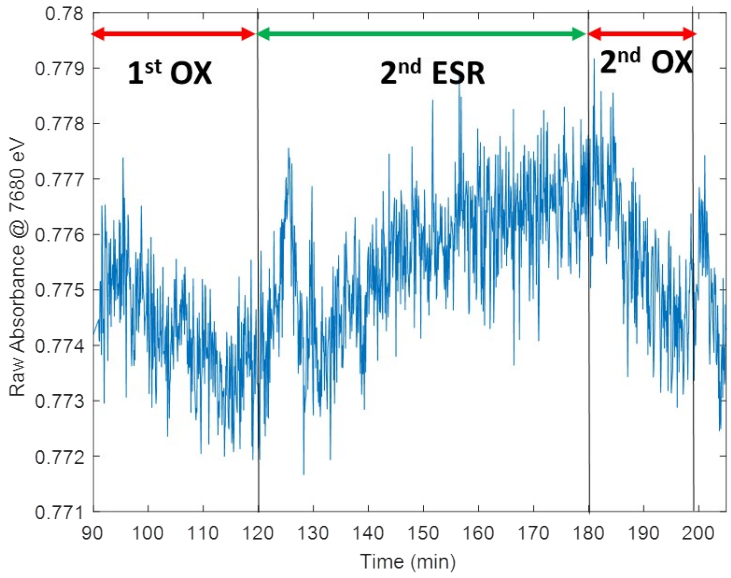

Fig. S6 Example of evolution of the raw absorbance at an energy position (7680 eV) before the rising edge where absorption is flat measured during OX-ESR-OX cycling. The decrease of raw absorbance observed during each oxidative condition (1st OX, 2nd OX) is indicative that the sample is more transparent to X-rays as expected if coke is burned in presence of O_2 atmosphere. At the opposite, a continuous increase of the absorption level is observed when the catalyst is only exposed to ESR gas feed (2nd ESR), related to the increase of coke deposits at the surface of the catalysts

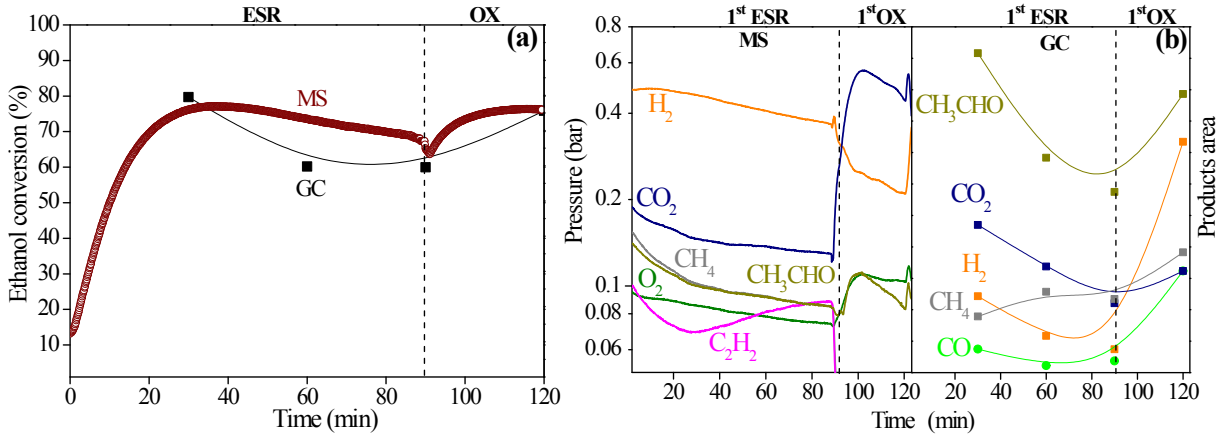

Fig. S7 The catalyst activity was also evaluated by GC during the 1st ESR and 1st OX in an independent experiment. The GC results are in agreement with the MS validating the catalyst performance measured by MS during the different cycling conditions. (a) Comparison of ethanol conversion and (b) products distribution determined by MS (logarithmic scale) and GC during the first ESR and subsequent 1st OX.

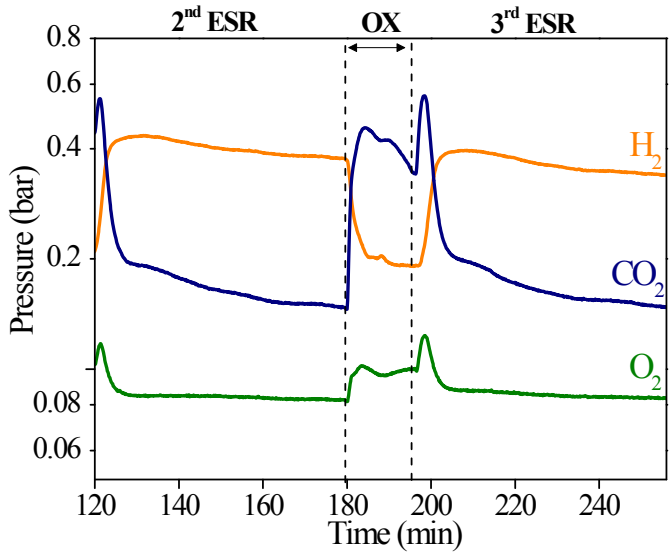

Fig. S8 Evolution of reaction products monitored by Mass Spectrometry during ESR-oxidative regeneration (OX) cycles.

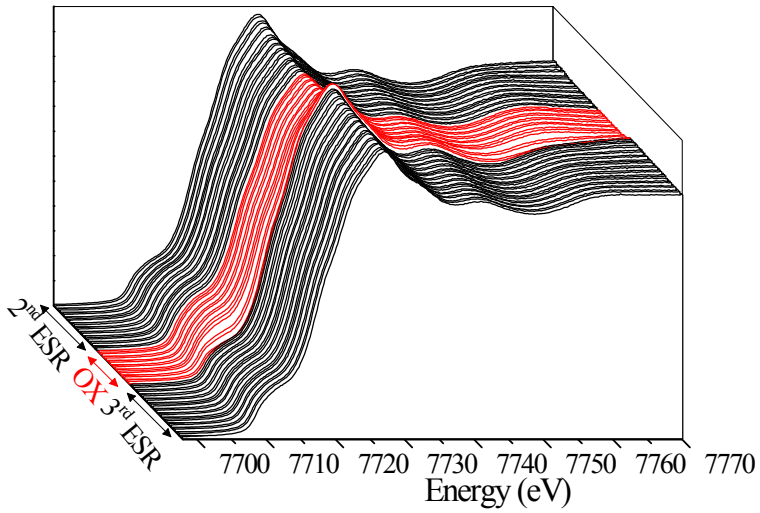

Fig. S9 Evolution of XANES spectra collected during ESR-oxidative regeneration (OX) cycles.

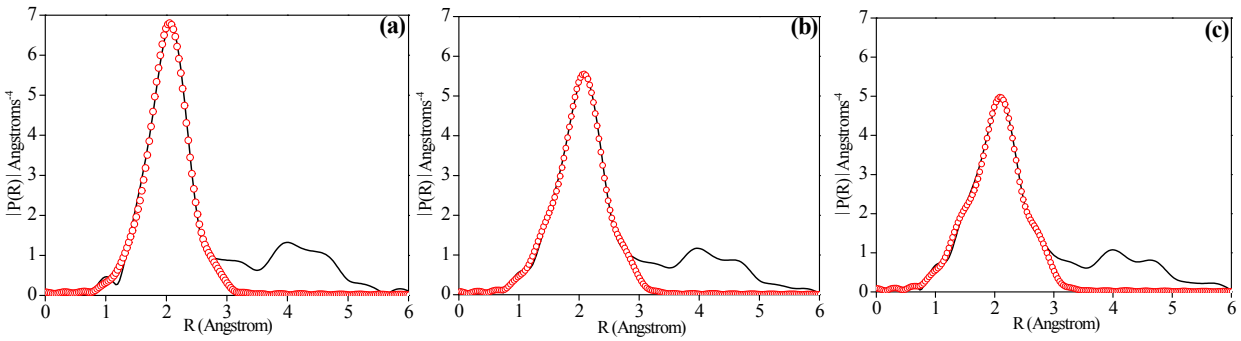

Fig. S10 Comparison of the results of least square fittings (dotted lines) with the magnitude of the Pseudo Radial Distribution Function (solid lines) obtained by the Fourier Transformation of the EXAFS spectrum measured at the end of the (a) first ESR, (b) second ESR and (c) third ESR.

Table S1. Best fitted EXAFS parameters of the Co/Al_2O_3 catalyst at the end of the different reactions. N: coordination number, R: atomic distance from the absorbing atom, σ^2: square of the Debye-Waller factor, energy shift. R_f measures the relative misfit of the theory with respect to the experimental spectrum. E_0=7709 ± 1.3 eV and the passive electron reduction factor S_0^2 = 0.75. Those values were determined first on references, such as the metallic foil, CoO and Co_3O_4.

		N	R (Å)	σ^2 (10^{-3} Å^2)	R_f
1st ESR	Co-Co (Co^0)	7.4 ± 0.4	2.46 ± 0.005	14	
	Co-O (CoO)	1.5 ± 0.3	1.95 ± 0.024	12	0.006
	Co-Co (CoO)	2.2 ± 0.9	2.98 ± 0.032	18	
2nd ESR	Co-Co (Co^0)	5.1 ± 0.3	2.46 ± 0.005	14	
	Co-O (CoO)	1.9 ± 0.3	1.96 ± 0.017	12	0.007
	Co-Co (CoO)	3.3 ± 0.8	2.98 ± 0.019	18	
3nd ESR	Co-Co (Co^0)	3.8 ± 0.3	2.46 ± 0.006	14	
	Co-O (CoO)	2.1 ± 0.3	1.95 ± 0.015	12	0.008
	Co-Co (CoO)	4.3 ± 0.8	2.98 ± 0.015	18	

* k-range = 3.30 - 11.0 Å^{-1} R-range = 1.0 - 3.05 Å

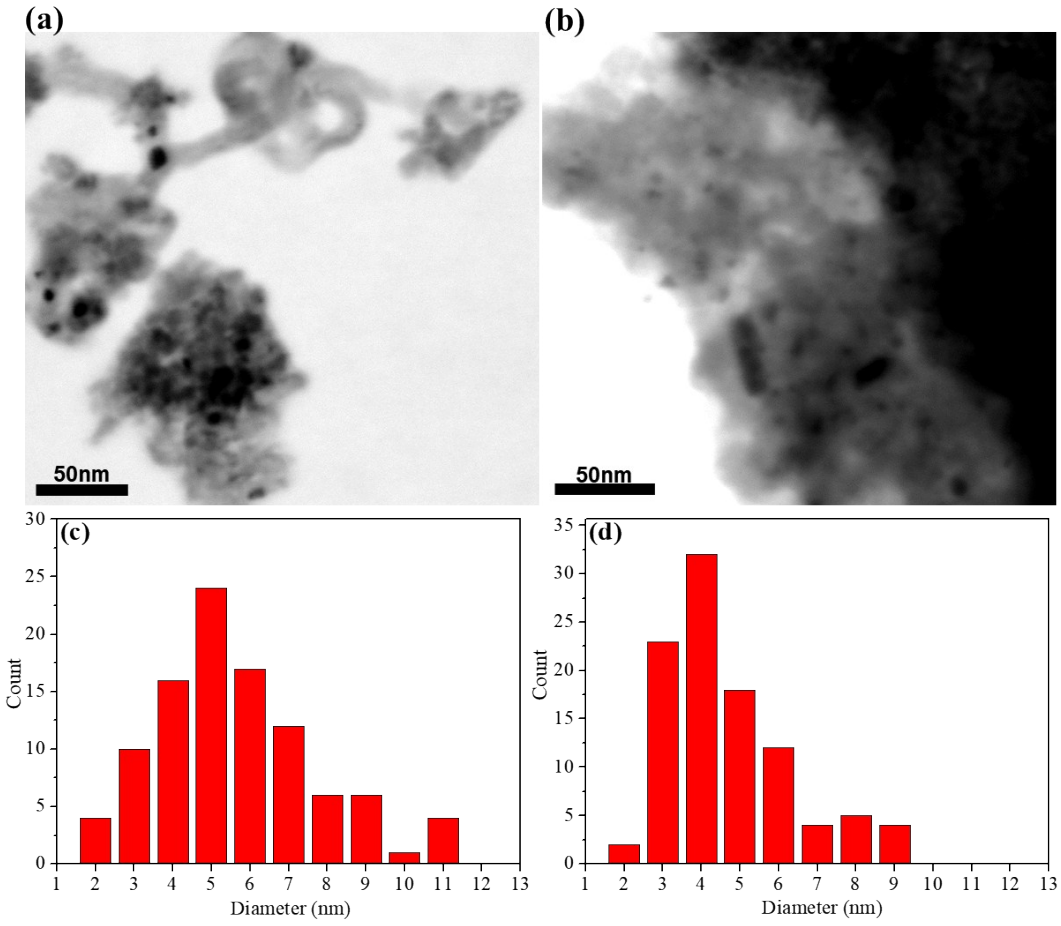

Fig. S11 (a) STEM images of the catalyst after the 1st ESR and (b) the 1st OX (c) size distribution after 1st ESR and (d) the 1st OX. After the 1st ESR, the presence of Co^0 nanoparticles with average size of 5.4 nm and carbonaceous deposits were observed. After 1st OX regeneration no carbon filaments were observed and the average size of cobalt decreases by 26% (4 nm). Those results are in agreement with the Raman results, and with the decrease of particle size estimated by Co-Co coordination number deduced from EXAFS fitting. It is important to note that in any case, particles in the 1nm range could be observed within the spatial resolution offered by the STEM microscope and only the few bigger ones have been observed. Despite the discrepancy in size determined by XAS (in the 1nm range) and STEM (around 4 to 5 nm) measurements, both techniques evidence that regeneration leads to a reduction of the cobalt particle sizes to smaller ones in the same proportion (~25%), validating our interpretation based on the Kirkendall effect.

Table S2. Proportion of cobalt species and coordination number determined by the fitting of the Co-Co first shell contribution of the Co K-edge EXAFS spectra of the catalyst at the end of each ESR cycle and related particle size

ESR-OX cycles	% Co^0	N_{Co-Co} (Co^0)*	Size (nm)
1st	89	8.3 (± 0.4)	1.2
2nd	74	6.9 (± 0.3)	0.9
3rd	67	5.7 (± 0.3)	0.7

* Coordination number rescaled by the %Co^0.

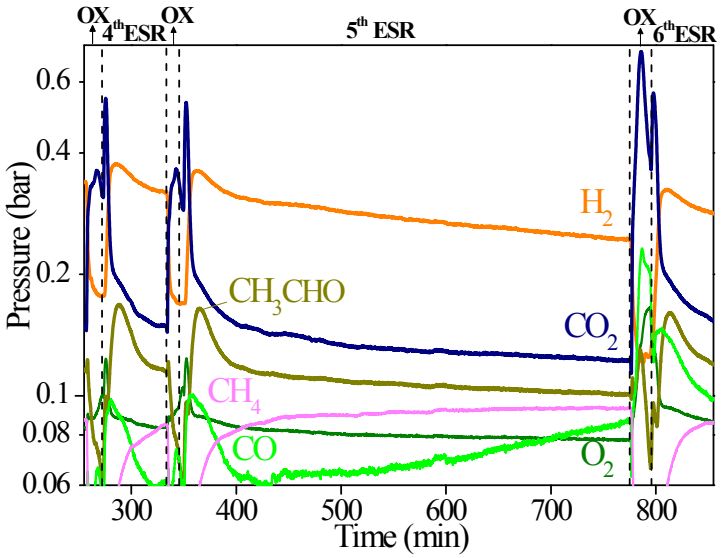

Fig. S12 Evolution of reaction products during 4th and 5th reaction-regeneration cycles.

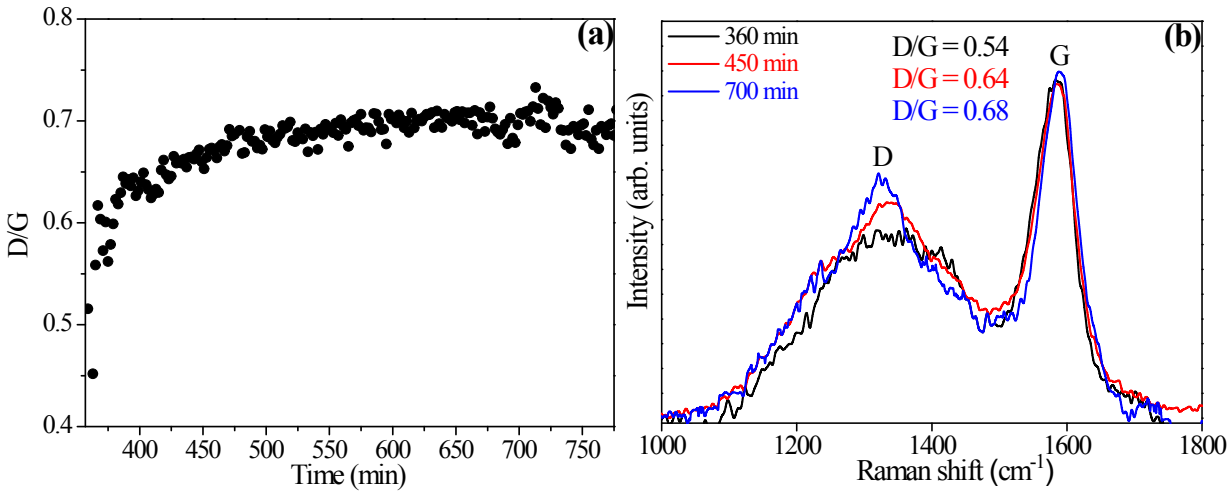

Fig. S13 (a) Evolution of the D/G Raman line intensity ratio during the 5th ESR and (b) Raman spectra measured at 360, 450 min and 700 min of the 5th ESR. For scaling the G line intensity, the spectrum measured at 700 min is multiplied by a factor 1.5. Actually, an overall reduction of the Raman signal is observed after 450 min. This reduction does not mean that coke is decreasing in quantity upon time but is related to a defocusing of the laser by swelling of the cell under coke formation. It is noteworthy that the D/G ratio is not modified by the laser defocusing since both lines suffer homothetic reduction of intensity. The laser defocusing is responsible for the decrease of the G line intensity observed Fig S2 and Fig. 5 in the time window 450-750 min.

References

1 C. La Fontaine, L. Barthe, A. Rochet and V. Briois, *Catal. Today*, 2013, **205**, 148–158.

2 V. Briois, C. La Fontaine, S. Belin, L. Barthe, T. Moreno, V. Pinty, A. Carcy, R. Girardot and E. Fonda, in *Journal of Physics: Conference Series*, 2016, vol. 712, pp. 012149–012155.

3 E. Fonda, A. Rochet, M. Ribbens, L. Barthe, S. Belin and V. Briois, *J. Synchrotron Radiat.*, 2012, **19**, 417–424.

4 C. Lesage, E. Dervers, C. Legens, G. Fernandes, O. Roudenko and V. Briois, *Submitted to Catalysis Today, special Issue of Operando VI.*

5 W. H. Cassinelli, L. Martins, A. R. Passos, S. H. Pulcinelli, C. V Santilli, A. Rochet and V. Briois, *Catal. Today*, 2014, **229**, 114–122.

6 A. Rochet, B. Baubet, V. Moizan, C. Pichon and V. Briois, *Comptes Rendus Chim.*, 2016, **19**, 1337–1351.

7 A. R. Passos, L. Martins, S. H. Pulcinelli, C. V Santilli and V. Briois, *ChemCatChem*, 2017, **9**, 3918–3929.

8 B. Ravel and M. Newville, *J. Synchrotron Radiat.*, 2005, **12**, 537–541.